

## Observations of Spheromak Equilibria Which Differ from the Minimum-Energy State and Have Internal Kink Distortions

S. O. Knox, Cris W. Barnes, G. J. Marklin, T. R. Jarboe, I. Henins, H. W. Hoida, and B. L. Wright

*Los Alamos National Laboratory, Los Alamos, New Mexico 87545*

(Received 11 June 1985)

Experimental spheromak magnetic equilibria are measured which differ significantly from the minimum-energy state, and are well described by a numerical model where  $j_{\parallel}/B$  has a linear dependence on the poloidal flux function. Equilibria are determined in a nonperturbing manner by the combination of measurements of flux-conserver image currents with calculations from this model. These equilibria are corroborated by the observation of nondisruptive rotating internal kink distortions (with toroidal mode numbers  $n = 1, 2,$  and  $3$ ), coupled with theoretical MHD thresholds for the onset of these modes.

PACS numbers: 52.55.Hc, 52.35.Py, 52.70.Ds

In a spheromak, the magnetic fields are generated primarily by internal currents rather than by external coils. Once established, these fields are conjectured<sup>1</sup> to relax towards a state of minimum energy subject to the constraint that the magnetic helicity<sup>2</sup> is conserved. In a closed system the minimum-energy equilibrium satisfies  $\nabla \times \mathbf{B} = \lambda \mathbf{B}$  with  $\lambda \equiv \mu_0 j_{\parallel}/B = \text{const}$ . Since competing effects are certainly present in any experiment, small deviations from a uniform, constant  $\lambda$  can be expected. However, these departures from the minimum-energy or "Taylor" state are expected<sup>1</sup> to relax towards this lowest-energy configuration on a time scale shorter than the resistive diffusion time.

We report results from the compact toroid experiment<sup>3,4</sup> (CTX) which give spheromak equilibria (determined in a nonperturbing manner) not with  $\lambda = \text{const}$ , but with  $\lambda = \lambda(\psi)$ , where  $\psi$  is the normalized poloidal flux function [ $\psi = (\text{poloidal flux value})/(\text{total poloidal flux})$ ]. The departures in magnetic energy of these equilibria with respect to the minimum-energy state is small. Coherent oscillations are seen, generated by rotating kink modes within the equilibria. The onset of the modes is shown to be consistent with the slope of  $\lambda(\psi)$  from the equilibrium measurement.

Other spheromak experiments<sup>5,6</sup> have measured the magnetic fields with internal probes, and have found experimental agreement with a zero-pressure, constant- $\lambda$  model. Hart *et al.*<sup>7</sup> obtained for their data better agreement by including a finite-plasma-pressure correction to a constant- $\lambda$  model.

In CTX, the  $\lambda(\psi)$  profile is inferred from external measurements of induced image currents flowing in a mesh flux conserver<sup>8</sup> (MFC) surrounding the plasma, combined with results from numerical calculations of the equilibrium. This general technique is in principle similar to that used before to establish the MHD equilibrium in noncircular-cross-section tokamaks [see, e.g., Luxon and Brown,<sup>9</sup> and references therein]. Application of the technique to the CTX spheromak benefits from increased sensitivity to equilibrium

changes since the spheromak is a small-aspect-ratio system; changes in the equilibrium affect the position of the magnetic axis and have a large effect on toroidal MFC image currents near the symmetry axis. Arrays of small Rogowski loops (5% relative calibration) measure the MFC currents, with the ratios of the currents (filtered to remove oscillations) at different radii used to determine the spheromak equilibrium. The present MFC, similar to but larger than the one outlined in Ref. 8, is approximately an oblate spheroid of diameter 136 cm and length 62 cm. It is constructed of 1.3-cm-diam oxygen-free, high-conductivity copper rods welded together at the rod crossings to form a mesh with a nominal spacing of 5 cm.

An axisymmetric ideal MHD equilibrium is computed by solution of the Grad-Shafranov equation, with the  $\lambda(\psi)$  profile and the boundary conditions specified. The plasma pressure is assumed to be zero. As a departure from a constant- $\lambda$  profile, we express  $\lambda$  by a power-series expansion in  $\psi$ , using only the first two terms:  $\lambda(\psi) = \bar{\lambda}[1 + \alpha(2\psi - 1)]$ , where the free parameter  $\alpha$  adjusts the slope of  $\lambda(\psi)$ . The coefficient  $\bar{\lambda}$  is the average of  $\lambda(\psi)$  over  $\psi$  and is determined by the geometry and  $\alpha$ . Each toroidal hoop of the MFC is assumed to be a perfect flux conserver, containing no net flux. In the model, all plasma currents are confined to the interior of the MFC. With use of these boundary conditions, the hoop image currents are then calculated as a function of  $\alpha$ . The best value of  $\alpha$  is obtained by application of a least-squares minimization technique to the difference between the measured and the calculated values of the toroidal-hoop currents as  $\alpha$  is varied. Knowing the value of  $\alpha$  specifies  $\lambda(\psi)$ , and the inverse rotational transform  $q(\psi)$  can then be calculated.

This procedure can be extended to include higher-order terms, either in the functional dependence of  $\lambda$  on  $\psi$ , or finite-plasma-pressure effects. Because the MFC is not a perfect flux conserver, a finite amount of equilibrium current ( $\sim 6\%$  of the spheromak po-

oidal current) flows in the poloidal hoops. This effect obscures the contributions of higher-order terms when they are included in the expression for  $\lambda(\psi)$ . Inclusion of plasma pressure in the numerical models does alter the MFC current distribution. But, for the pressures of similar CTX discharges ( $\beta_{\text{peak}}$  of 6% from Thomson scattering and interferometry), the effect is smaller than the error of the present method. The dominant effect on the MFC currents is the zero-pressure  $j_{\parallel}/B$  distribution. Thus, within the accuracy of the measurements, a linear approximation to  $\lambda(\psi)$  provides a quantitative as well as qualitative explanation of the experimental observations.

The evolution of a typical CTX discharge has two phases: the formation and sustainment phase when magnetic helicity is injected to build up and maintain the spheromak fields, and the resistive-decay phase which begins when the helicity source is turned off. One representative discharge has been selected for detailed analysis here. The spheromak was formed by a magnetized coaxial plasma source operating with a current wave form that was approximately a square pulse between 0.1 and 0.7 ms. The peak toroidal plasma current at 0.7 ms was 420 kA,  $B_{\text{max}} = 5.6$  kG, and  $\langle n_e \rangle = 9 \times 10^{13} \text{ cm}^{-3}$ . Beginning at 0.7 ms, the spheromak plasma current resistively decayed until it terminated at 1.55 ms.

Figure 1(a) shows examples of two MFC toroidal currents at the same toroidal angle but at two poloidal positions, one near the symmetry axis and one near the maximum radius of the flux conserver. (The oscillations apparent in Fig. 1 are discussed below.) Throughout formation and sustainment the ratio of the filtered currents remains nearly constant. As the equilibrium changes from the sustainment to the decay phase, the magnetic axis moves radially outward, and the distribution of the toroidal MFC currents changes, with the MFC currents near the symmetry axis decaying more rapidly than those near the outside midplane.

Figure 2 is a summary of the time evolution of the equilibrium. The solid symbols of Fig. 2(a) are the experimental values for the MFC toroidal-hoop current ratios, and the solid lines plus shading are the theoretical current ratios which form a reasonable confidence interval on the value of  $\alpha$ . The value of  $\alpha$  which gives the best fit to the experimental data is indicated. Using the best-fit values for  $\alpha$  ( $\pm \Delta\alpha = 0.05$  error), the corresponding  $\lambda(\psi)$  and  $q(\psi)$  ranges for a particular equilibrium are then calculated [Figs. 2(b) and 2(c), respectively]. During the sustainment phase (0.1–0.7 ms) while helicity is injected, the  $\lambda(\psi)$  profile [cf. Fig. 2(b)] is peaked towards the outside of the spheromak ( $\psi \rightarrow 0$ ), indicating a relatively high value of  $j_{\parallel}/B$  in that region. This is consistent with the interpretation of spheromak sustainment by currents driven primarily on the outer flux surfaces. The CTX experiment has

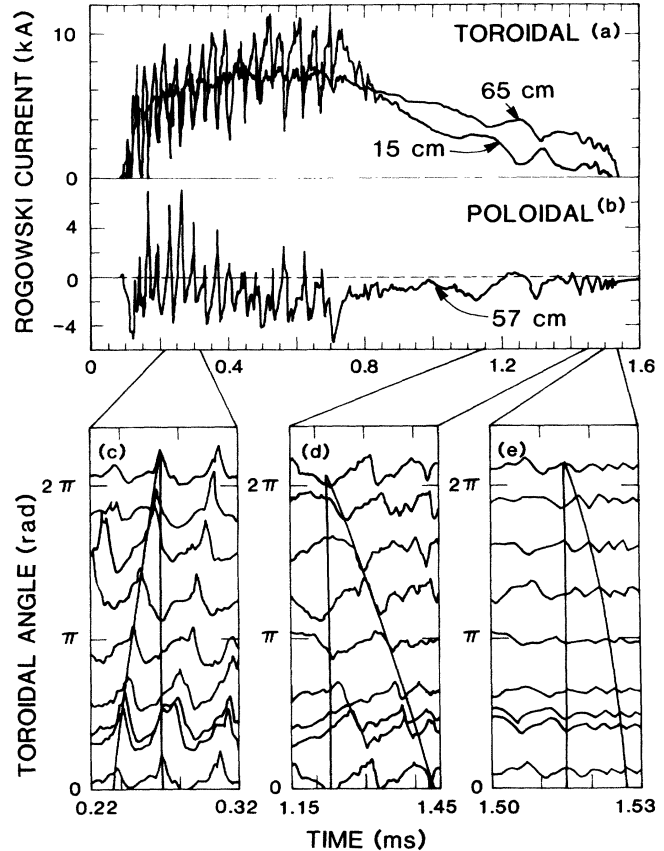


FIG. 1. (a),(b) Representative MFC currents. Indicated lengths are the radial distances from the symmetry axis to the MFC hoops. (c)–(e) Toroidal-mode-number analysis. Poloidal MFC currents at eight toroidal locations (same radius) are displayed. The curved phase fronts ( $n=2,3$ ) show the increasing rotation frequency.

maintained this non-minimum-energy equilibrium during sustainment for up to 6 ms (greater than ten magnetic-energy decay times). In the next time interval (0.8–1.05 ms), no oscillations are present and the  $\lambda(\psi)$  profile is essentially independent of  $\psi$ . At this time the equilibrium has a  $\lambda$  profile very near the minimum-energy or Taylor state. The spheromak does not remain in this state, nor does it return during the remainder of the resistive-decay phase of the plasma. During the following time interval (1.1–1.3 ms), the  $\lambda(\psi)$  profile continues to change slope with resistivity gradients causing  $j_{\parallel}/B$  to peak towards the magnetic axis ( $\psi \rightarrow 1$ ), resulting in a further drop in  $q$ . The peaking continues during the next time interval (1.45–1.55 ms), where the  $\lambda(\psi)$  slope increases even further. The configuration then terminates when the particle density goes to zero.

These linear  $\lambda(\psi)$  profiles are substantiated by the manifestation of rotating internal kink distortions<sup>6,10</sup> as coherent oscillations in the MFC currents. We first

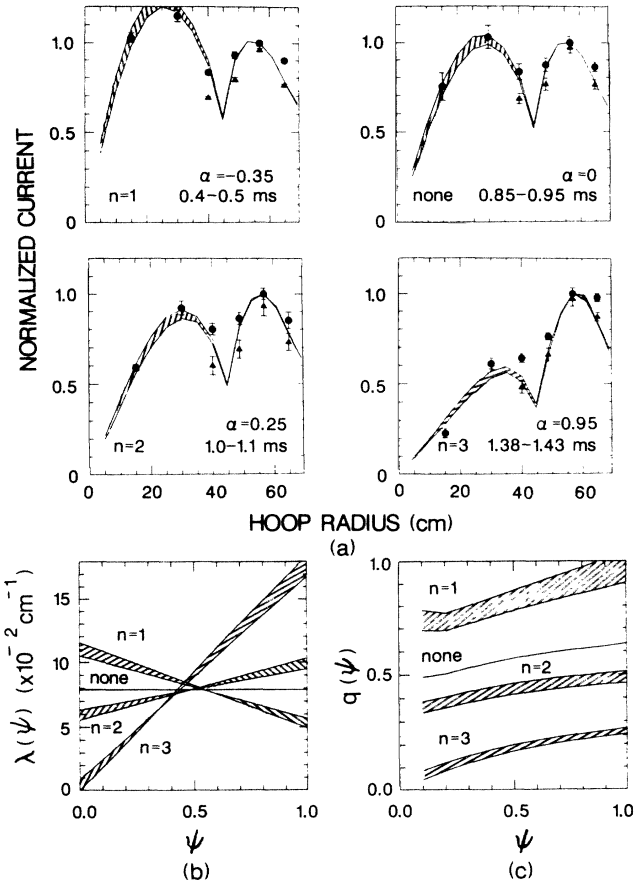


FIG. 2. Time evolution of the equilibrium. (a) Experimental values (circles, from hoops on the MFC "hemisphere" away from entrance region; triangles, from the MFC hemisphere toward the entrance region) and theoretical MFC toroidal-hoop current ratios (solid lines) for the indicated averaging times. The sharp minima correspond to the corners of the MFC. Experimental data are normalized to the value at hoop radius of 56.8 cm, on the side away from the entrance region. (b)  $\lambda(\psi)$  vs  $\psi$  profiles for (a). Curves are identified by the dominant toroidal mode number,  $n$ , at that time. (c)  $q(\psi)$  vs  $\psi$  profiles for (a).

describe the modes, and then couple their occurrence (first in the experiment and then in a stability analysis) to  $\lambda(\psi)$  via the slope parameter  $\alpha$ . The primary toroidal mode number,  $n$ , of the oscillations can be determined by examination of the toroidal phase of the poloidal MFC currents. In Fig. 1(c), as the phase of the mode rotates once in the positive toroidal direction, the oscillation goes through one cycle, and hence is primarily an  $n=1$  mode. During the decay phase of the discharge, modes with higher toroidal mode numbers appear. First an  $n=2$  mode appears [Fig. 1(d)], and then near the end of the discharge an  $n=3$  mode becomes the primary oscillation [Fig. 1(e)]. The rotation of the  $n=1$  mode during formation is driven by an  $\mathbf{E} \times \mathbf{B}_p$  drift applied by the gun voltage; the mode

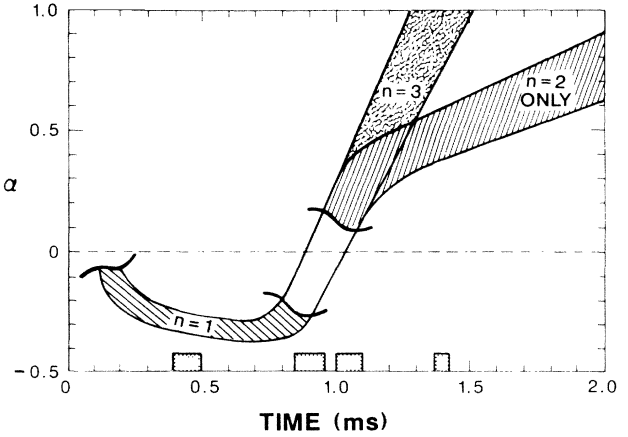


FIG. 3. Experimental trajectory of the  $\lambda(\psi)$  slope parameter  $\alpha$  vs time. Times indicated at the bottom correspond to the equilibria of Fig. 2.

rotation direction reverses when either the polarity of the voltage or the poloidal field of the spheromak changes direction, and the frequency of rotation is proportional to the applied voltage. The decaying spheromak modes ( $n=2,3$ ) rotate in the direction of the toroidal electron diamagnetic drift; the rotation direction reverses when the poloidal field is reversed, but not when the toroidal field is reversed. The presence of the oscillations is not disruptive to the equilibrium. In a typical discharge, the ratio  $\Delta B_p/B_p$  (as inferred from surface-averaged measurements of  $\Delta I_t/I_t$  in the MFC) reaches a steady-state value of 6%–8% during the sustainment phase, drops to 2%–3% during the time of no oscillation, and then saturates at 9%–11% when the  $n=2,3$  modes are present.

A convenient visualization of the  $\lambda(\psi)$  evolution is a plot of the slope parameter  $\alpha$  versus time, as shown in Fig. 3. The shaded band is the range of  $\alpha(t)$  for discharges which develop an  $n=3$  mode, and the crosshatched area is for a set of discharges with higher plasma density which develop only an  $n=2$  mode in the decay phase. For the former case (shaded),  $\alpha \approx -0.3$  during the sustainment phase, passes through zero (minimum-energy state), and then continues to increase for the remainder of the discharge. However, the  $\alpha(t)$  trajectory for discharges with only  $n=2$  modes is different, as the  $\alpha(t)$  trajectory rolls over at  $\alpha \approx 0.5$ ; that is, the  $\lambda(\psi)$  slope does not continue to increase as rapidly in time. The transport properties of these discharges (formed at higher filling pressure<sup>4</sup>) reduce the rate at which  $j_{||}/B$  continues to peak towards the magnetic axis, and the spheromaks do not become  $n=3$  unstable.

The  $\alpha$  parameter is used to compare thresholds from a linear ideal MHD stability analysis with the occurrence of the observed unstable modes. The growth

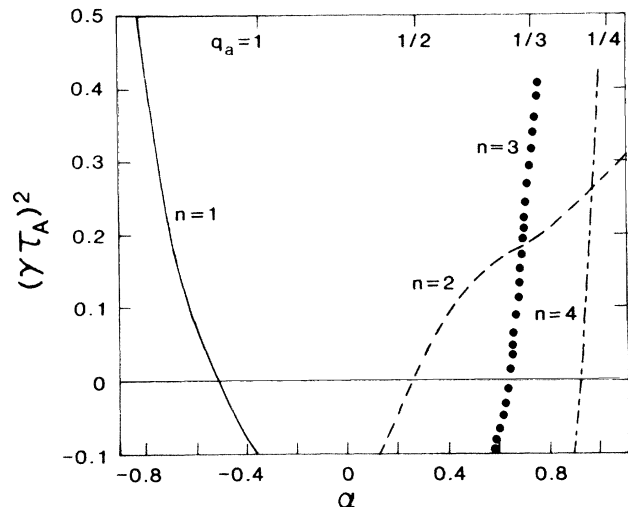


FIG. 4. Square of the normalized toroidal mode growth rate vs  $\alpha$  from linear ideal MHD stability analysis. Values are normalized to the Alfvén transit time  $\tau_A = R/\langle V_A \rangle$ , where  $\langle V_A \rangle = (\int B^2 dv / \mu_0 \int \rho dv)^{1/2}$  is the volume-averaged Alfvén speed. The value of  $q_a$  is given at the top of the figure.

rate  $\gamma_n$  for the fastest-growing toroidal mode number  $n$  is determined as a function of  $\alpha$ . The square of this growth rate is plotted in Fig. 4 for the  $n=1, 2, 3$ , and 4 modes. Figure 4 shows the  $n=2$  mode becoming unstable when  $\alpha$  is 0.25 and the  $q(\psi)$  at the magnetic axis,  $q_a$ , is approximately  $\frac{1}{2}$ . The  $n=3$  mode takes over when  $\alpha \approx 0.7$  and  $q_a \approx \frac{1}{3}$ . These values of  $\alpha$  agree with the appearance of the  $n=2$  and  $n=3$  modes in the experiment (see Figs. 2 and 3). The  $n=1$  ideal MHD mode, however, does not become unstable until  $\alpha \approx -0.5$  and  $q_a$  is substantially above 1. The experimentally observed  $n=1$  mode, which appears when  $\alpha \approx -0.3$  and  $q_a \approx 1$ , is probably the result of a resistive instability with a lower threshold.

The internal kink modes, which are driven unstable by the  $\lambda(\psi)$  profile, do not cause a full relaxation of the spheromak back to the minimum-energy state. The transport processes which cause  $j_{||}/B$  peaking towards the magnetic axis are not balanced by the stabilizing influence of multiple reconnections, which make possible a redistribution of the current, as in the reversed-field pinch.<sup>11</sup> This nonrelaxing behavior of the decaying spheromak modes is similar to that seen in a numerical simulation of nonresonant spheromak

modes,<sup>12</sup> where internal ideal MHD modes grew to small but finite amplitude, resulting in a smooth transition to a new helical equilibrium.

In summary, because of nonuniform resistivity, spheromak equilibria as described by a linear dependence of  $\lambda$  on  $\psi$  are found to pass monotonically through the minimum-energy state, and are observed to maintain departures from the minimum-energy profile for times greater than the resistive decay time of the configuration. Deviations from the exact minimum-energy state apparently do not require a concomitant relaxation. These deviations are small in terms of free magnetic energy relative to the Taylor minimum-energy state, as  $(W_B - W_{\text{Taylor}})/W_{\text{Taylor}} \leq 0.1$  for  $|\alpha| \leq 0.7$ . Spheromak equilibria are determined by the combination of measurements of flux-conserver image currents with a numerical model, and an example of the evolution of a CTX spheromak showing  $\lambda(\psi)$  and  $q(\psi)$  versus time is given. Associated with the slope of  $\lambda(\psi)$  is the occurrence of rotating internal kink modes, with toroidal mode numbers  $n=1, 2$ , and 3 at different times during the discharge. The amplitudes of these oscillations during any phase of the discharge saturate with  $\Delta B_p/B_p \leq 11\%$ .

We wish to thank A. R. Sherwood for a careful reading of the manuscript and R. Scarberry for the construction of the Rogowski loops. This work is supported by the U. S. Department of Energy.

<sup>1</sup>J. B. Taylor, Phys. Rev. Lett. **33**, 1139 (1974).

<sup>2</sup>H. K. Moffatt, *Magnetic Field Generation in Electrically Conducting Fluids* (Cambridge Univ. Press, New York, 1978).

<sup>3</sup>T. R. Jarboe *et al.*, Phys. Rev. Lett. **51**, 39 (1983).

<sup>4</sup>C. W. Barnes *et al.*, Nucl. Fusion **24**, 267 (1984).

<sup>5</sup>W. C. Turner *et al.*, Phys. Fluids **26**, 1965 (1983).

<sup>6</sup>A. Janos *et al.*, Phys. Fluids **28**, 3667 (1985).

<sup>7</sup>G. W. Hart *et al.*, Phys. Rev. Lett. **51**, 1558 (1983).

<sup>8</sup>T. R. Jarboe *et al.*, Phys. Fluids **27**, 13 (1984).

<sup>9</sup>J. L. Luxon and B. B. Brown, Nucl. Fusion **22**, 813 (1982).

<sup>10</sup>T. R. Jarboe *et al.*, in *Proceedings of the Tenth International Conference on Plasma Physics and Controlled Nuclear Fusion Research, London, 1984* (International Atomic Energy Agency, Vienna, 1985), Vol. 2, p. 501.

<sup>11</sup>E. J. Caramana *et al.*, Phys. Fluids **26**, 1305 (1983).

<sup>12</sup>W. Park and S. C. Jardin, Phys. Fluids **26**, 1871 (1983).

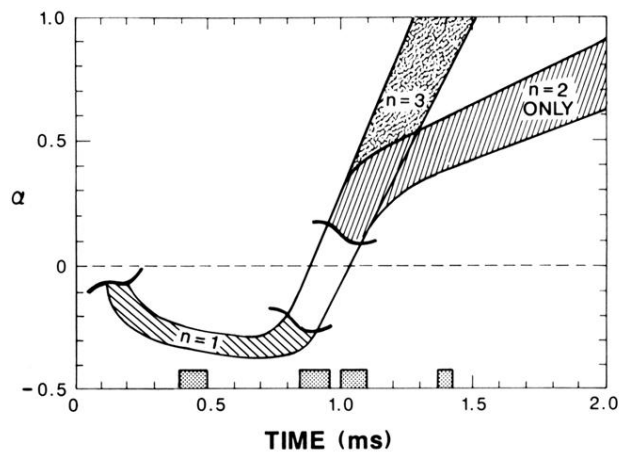


FIG. 3. Experimental trajectory of the  $\lambda(\psi)$  slope parameter  $\alpha$  vs time. Times indicated at the bottom correspond to the equilibria of Fig. 2.